View metadata, citation and similar papers at core.ac.uk

brought to you by CORE

provided by eCommons@Cornell

LOAD BEARING CHARACTERISTICS OF IMPLANTS FOR OSTEOCHONDRAL DEFECT REPAIR

A Thesis

Presented to the Faculty of the Weill Cornell Graduate School

of Medical Sciences

in Partial Fulfillment of the Requirements for the Degree of

Masters in Clinical & Translational Investigation

by

Tony Chen, PhD

August 2015

© 2015 Tony Chen

ABSTRACT

Objective: To measure changes in joint contact mechanics, during simulated gait, in the presence of a medial femoral osteochondral defect and after filling the defect using two different polyvinyl alcohol implant configurations.

Methods: Seven human cadaveric knees were tested under simulated gait, while the contact stresses on the tibial plateau were recorded using an electronic sensor. Each knee was tested using the following conditions: intact, defect, and after the defect has been filled with either 10% PVA, 20% PVA, 10% PVA + a porous titanium base, or 20% PVA + porous titanium base. Changes in contact area, total force, weight center of contact, and stress pattern differences were measured for each knee.

Results: At 14% of the gait cycle, there were no changes in contact area observed between conditions. At 45% of the gait cycle, differences were seen in the meniscal-cartilage contact area with increases in contact area between the intact and 10% PVA as well as 20% PVA scaffolds. At 14% of gait, there was a significant increase in total force between intact and defect conditions and between defect and 20% PVA + pTi in the menical-cartilage region with forces of 179 ± 113 N, 278 ± 113 N, and 193 ± 96 N for the intact, defect, and 20% PVA + pTi respectively. At 45% of gait, there was a significant difference in total force between intact condition and the defect condition in the meniscal-cartilage contact area with average total force of 90 ± 73 N and 148 ± 75 N respectively. Differences were found in the cartilage-cartilage total force at 45% of gait between intact and all other conditions and between defect and 20% PVA + pTi. The total forces were 486 ± 134 N for the intact, 360 ± 158 N for the defect, and 431 ± 177 for the 20% PVA + pTi, and the remaining implants tested having total force values below 412 N.

Conclusions: The presence of an osteochondral defect causes an increase in loading on the meniscus. Implants in the range of tissue engineered constructs can partially restore joint loading but cause alterations in contact stress patterns.

BIOGRAPHICAL SKETCH

The author was born in Charlottesville, Virginia on November 16th, 1981. He attended the University of Pennsylvania from 2000 to 2004, and graduated with a Bachelor of Science in Engineering degree in 2004. He came to the University of Rochester in the Fall of 2004 and began graduate studies in the Department of Biomedical Engineering. He pursued his research in Cartilage Tissue Engineering at the Musculoskeletal Tissue Engineering Laboratory in The Center for Musculoskeletal Research under the direction of Professor Hani A. Awad and received the Master of Science degree from the University of Rochester in 2005. The author went to on receive his Doctorate in Biomedical Engineering from the University of Rochester in 2010 afterwhich, he began his post-doctoral fellowship at the Hospital for Special Surgery in the Department of Biomechanics and is currently a Research Associate at the hospital.

ACKNOWLEDGMENTS

The author would like to acknowledge the contributions of Caroline Brial, MS; Moira McCarthy, MD; Hongsheng Wang, PhD in the collection of data in this work. Research reported in this publication was supported by the National Institute of Arthritis and Musculoskeletal and Skin Diseases, part of the National Institutes of Health, under Award Number R01 AR057343. The content is solely the responsibility of the authors and does not necessarily represent the official views of the National Institutes of Health. Funding was also received from KL2RR000458 of the NIH funded Clinical and Translational Science Center at Weill Cornell Medical College.

TABLE OF CONTENTS

LIST OF FIGURES

INTRODUCTION

Focal articular cartilage defects pose a serious socio-economic problem, in the form of stiff painful joints which are subsequently at high risk for the development of early osteoarthritis [1, 2]. These defects affect approximately 16% of the general population and 36% of the athlete population [3]. In simplified biomechanical models, the presence of focal defects have been shown to cause an increase in contact stresses around the periphery of the defect [4], which can lead to further degeneration of the surrounding tissue. To prevent further degeneration of the articular cartilage, attempts are made to fill the defects [5], but all current clinical treatment methods are prone to failure due in part to differences in material properties between the repair and host tissue, and difficulties with achieving robust host integration [6]. Therefore, there has been recent interest in developing tissue engineered scaffolds and synthetic implants for the repair of these focal defects. These systems include the use of bioreactor grown tissues [7-11], biphasic scaffolds [12-15], and non-degradable implant systems [16-19].

The goal of tissue engineered and synthetic implant materials intended for the treatment of osteochondral defects is to restore the continuity of the joint surface thus restoring the distribution of loads. While it has been shown that tissue engineered and synthetic implants can be created with mechanical properties within the range of articular cartilage, the ability of these implants to restore the distribution of loads to that of the intact condition remains unclear. Indeed, the effect of cartilage defects on the contact stresses of knees when subjected to dynamic activities of daily living has not yet been quantified, and this lack of knowledge has led to a situation whereby the true

mechanical consequences of the defects are unclear, and the functional assessment of implants intended to treat the defect is impossible. We have developed a unique cadaveric model capable of applying physiological loads across human cadaveric knees [20-22]. By combining this model with contact stress sensors, we can assess the effect of focal defects and implant repairs on the contact mechanics of the knee.

To test the ability of different repairs to restore normal joint contact mechanics, we used a novel polyvinyl alcohol (PVA) implant with and without the addition of a porous titanium base (pTi) added to simulate biphasic scaffold systems. The properties of PVA can be controlled by the number of freeze-thaw cycles and concentration of polymer [23]; making it an ideal test system for simulating the range of mechanical properties reported for scaffolds and implants for osteochondral defect repair. The objectives of this study are to: (i) understand the biomechanical consequences of a focal defect in human knees subjected to physiological loads that replicate the activity of gait, and (ii) characterize the ability of implants, as a function of their structural stiffness and composition, to restore the distribution of loads across the joint surface compared to that of the intact condition.

METHODS

Cadaveric Knee Preparation

Approval for use of cadaveric specimens was obtained from the Institutional Review Board of the Hospital for Special Surgery. Eight cadaveric knees were selected for experimental testing using the following exclusion criteria: no previous history of

osteoarthritis, diabetes, and traumatic injuries. The knees were prepared as described in Gilbert, et al. [21]. Briefly, the specimens were carefully stripped of soft tissue ensuring that the capsule, cruciate ligaments, collateral ligaments, and menisci remained intact. The knees were then pinned through the epicondylar axis using a 2.5 mm Kirschner wire to define the flexion axis. The axis was verified using anterioposterior and lateral fluoroscopic images before potting the knees in the simulator.

Simulator Setup

A Stanmore Knee Simulator was modified with custom designed fixtures to accept cadaveric knees [20] and depicted in Figure 1A. For each knee, the tibia was cut to fit into the tibial pot of the simulator such that the epicondylar pin placed in the knee was aligned with the flexion axis of the simulator. The tibia was fixed into the pot using polymethyl methacrylate (PMMA). Once the tibia was fixed in place, the epicondylar pin was removed and the femur was fixed in the femur pot of the simulator using PMMA. The simulator is an open-loop system and as such, the system must be adjusted until the outputs from the load cells and potentiometers of the simulator match the simulator inputs before testing can proceed.

Contact Stress Measurement

Contact stress normal to the surface of the tibial plateau was measured using a thin electronic sensor (Tekscan 4011; South Boston, MA) that consists of two independent sensor arrays (Figure 1B). The sensor was augmented with tabs to allow for attachment to the surrounding soft tissue and sealed using Tegaderm^{TM} (3M; St Paul, MN) to protect the sensors from fluid damage in the joint space. Cuts of 1 cm in length

were made in the anterior and posterior meniscal capsular attachments to provide entry points for the sensor. The sensor was placed on the tibial plateau of both the medial and lateral sides and anchored into the anterior footprint of the ACL and posterior capsule using 2-0 ethibond sutures (Ethicon; Somerville, NJ). Each sensor array consists of a matrix of 21 x 13 sensing elements, hereafter called sensels, with each sensel covering a 2 x 2 mm area. The sensors were programmed to record the contact stress across the sensor at a frequency of 100 Hz for 40 seconds.

Knee testing

The Stanmore Knee Simulator was used to control the axial force, anterior-posterior force, internal-external torque and flexion-extension profiles (Figure 1C) to mimic the activity of walking (Figure 1D), as per the guidelines from the International Standards Organization (ISO #14243-1) [24].

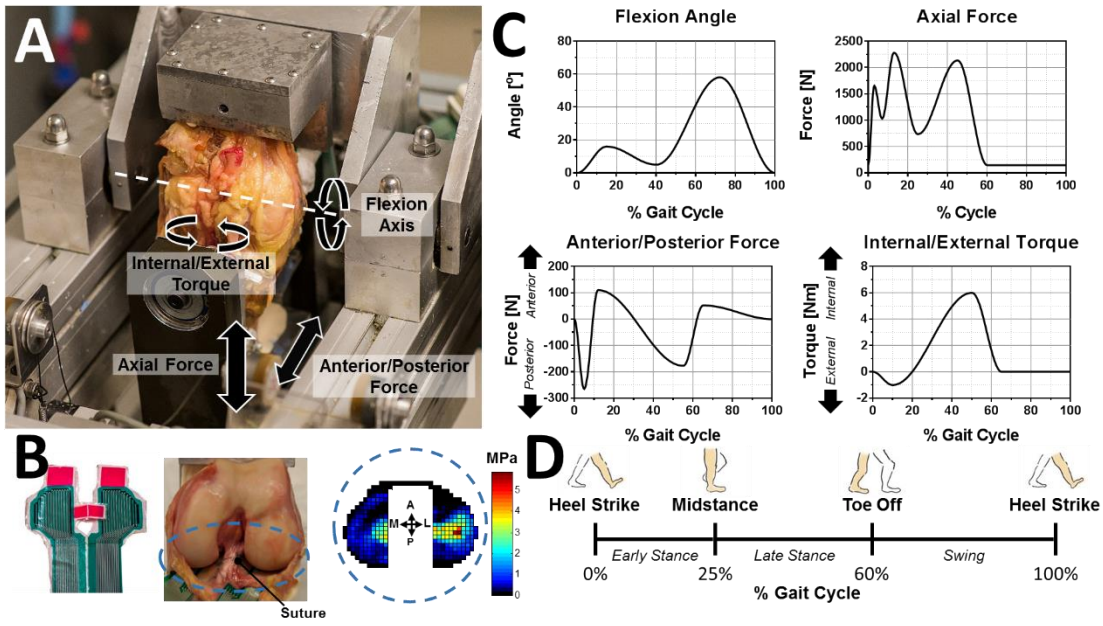

Figure 1: *Experimental Cadaveric Setup.* A) A Stanmore knee simulator was adapted to apply dynamic simulated gait to cadaveric knees. B) A Tekscan sensor was sutured into place on the tibial plateau of the knees to measure changes in contact stress. C) Inputs to simulate the D) different portions of the gait cycle.

The knees were first tested intact. Subsequently, the knees were flexed and a defect was created on the medial femoral condyle using an 8 mm Arthrex low profile reamer (Naples, FL) to a depth of 10 mm. The location of the defect was standardized using a series of measurements of the femur and medial condyle (Figure 2) which was determined in 3 pilot knees. The implant conditions were tested after the defect is drill; randomizing the order of the PVA and PVA + pTi conditions. The implants were removed and the knee was tested with the defect empty. The defect conditions were always tested last to protect the sensor from failing due to high shear stresses caused by the edge of the empty defect.

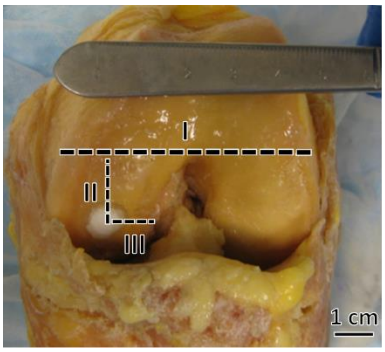

Figure 2: *Standardization of Osteochondral Defect Location.* A horizontal line, I, was drawn across the width of the femur tangential to the inter-condylar notch. A second line, II, perpendicular to I is drawn down the medial condyle 0.26 the length of I. The third line, III, was drawn perpendicular to II with a length that is 0.18 the length I.

Implant Manufacture

PVA implants were created using 10% or 20% PVA to generate constructs with an elastic modulus of 40 and 140 kPa [18], in the range of tissue engineered constructs. Implants were created by pouring either 10% or 20% liquid PVA into 100 cm^2 tissue culture dishes. The PVA then underwent 6 freeze/thaw cycles. After the completion of the freeze/thaw cycles, 8 mm diameter implants were cored from the polymerized PVA in the dishes. In the case of the implants consisting of PVA alone, the implants were shaved to 10.2 mm in height using a sledge microtome. For implants consisting of PVA + pTi, liquid PVA was added to the surface of the pTi and the PVA implant was attached to the pTi. The biphasic implant then undergoes another 3 freeze/thaw cycles before testing and also have a final height of 10.2 mm. Of note, the height of the implants cause them to protrude 0.2 mm above the surface of the cartilage. The extra 0.2 mm of height was added to the implants as it was observed in the pilot testing that this provided the best load bearing properties for the implants without causing the PVA to fail in shear.

Stress Pattern Difference Maps

The differences in contact pattern at each sensel between conditions was quantified using normalized cross correlation (NCC). The NCC was calculated using the following equation:

$$NCC = \frac{\sum_{t=u}^{t_N=u+N-1} \left(f(t) - \bar{f}_u\right)\left(t\left(t-u\right) - \bar{t}\right)}{\sqrt{\sum_{t=u}^{t_N=u+N-1} \left(f(t) - \bar{f}_u\right)^2 \sum_{t=u}^{u+N-1} \left(t\left(t-u\right) - \bar{t}\right)^2}} \qquad \textit{eq. 1}$$

where t is the time (seconds), u is the time for one full gait cycle (2 seconds), N is the current time shift, f is the function describing the pattern of interest, $\bar{f}$ is the mean of the current time window, τ is the template function, $\bar{\tau}$ is the mean of the current template function.

The normalized cross correlation gives a value between 0 and 1, where 0 denotes that compared patterns are not the same (Figure 3A) and 1 denotes that the patterns are exactly the same (Figure 3B). This form of cross correlation does not take into account magnitude differences between conditions and is therefore only an indication of differences in the pattern of the loading cycle itself. The total pattern difference on the medial and lateral plateau was calculated for each condition and compared to the intact condition.

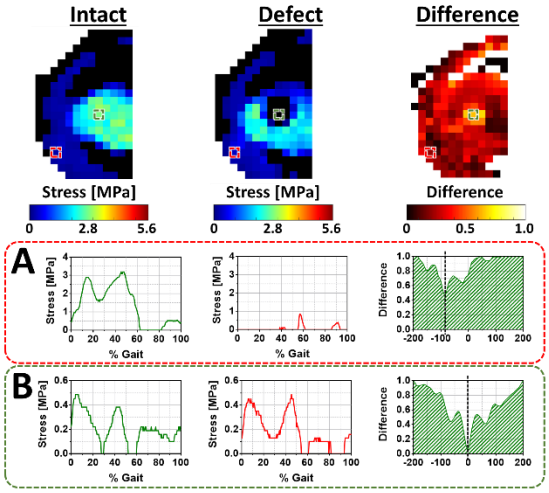

Figure 3: *Example Pattern Differences.* Sensels with a A) high and B) low pattern difference are shown for a representative knee. The pattern difference map is generated by calculating the pattern difference at each sensel on the sensor. Colored dotted boxes on the intact, defect, and difference maps correspond to stress patterns given in A and B.

Data Analysis

Analysis of data was performed only on contact stress data collected on the medial plateau on 7 out of the 8 knees due to 1 knee fracturing during testing. Regions of interest (ROI) were drawn to separate regions of meniscal-cartilage and cartilage-cartilage contact, Figure 4A&B, using the contact stress maps at 14% of the gait to identify the footprint of the meniscus. The ROIs were kept static throughout the gait cycle and between test conditions. Contact area and total stress were calculated for each of the ROIs.

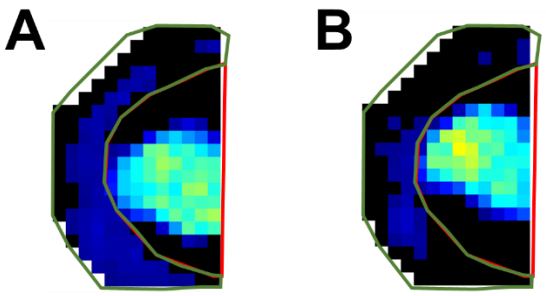

Figure 4: *Example of Separation of the Medial Tibial Plateau into Meniscal-Cartilage and Cartilage-Cartilage Contact Regions.* An example of regions of interest from a representative knee around areas of meniscal-cartilage (green) and cartilage-cartilage (red) contact at A) 14% and B) 45% of gait.

The weighted center of contact stress (WCoCS) was calculated as previously described [21]. The WCoCS was used to quantify shifts in contact stress in the medial/lateral (M/L) and anterior/posterior (A/P) directions in the presence or absence of a focal articular cartilage defect and with the different stiffness implants.

Statistical Analysis

The conditions were compared using a two-way analysis of variance (ANOVA) to identify differences in contact area and contact stress between the tested conditions at 14% and 45% of gait. Tukey post-hoc testing was performed to determine differences between conditions. Two-way ANOVA was also used to identify differences in the WCoCS over time, with Tukey post-hoc testing performed to determine differences between conditions. The difference in the means was considered significant when $p<0.05$. Total pattern differences between conditions were also identified using two-way ANOVA comparing between medial and lateral as well as between conditions.

RESULTS

Contact Area on the Medial Plateau

The contact area in the meniscal-cartilage and cartilage-cartilage ROIs were compared at 14% and 45% of the gait cycle. At 14% of the gait cycle, there were no differences in the meniscal-cartilage contact area (Figure 5A) or cartilage-cartilage contact area (Figure 5B) between conditions. At 45% of the gait cycle, differences were seen in the meniscal-cartilage contact area with increases in contact area between the intact and 10% PVA as well as 20% PVA scaffolds, with contact areas of 212 ± 78 mm^2, 263 ± 45 mm^2, and 281 ± 54 mm^2 respectively (Figure 5A). No differences were seen in the contact area in the cartilage-cartilage ROI at 45% of gait (Figure 5B).

Total Force on the Medial Plateau

Differences were found between intact and defect, and defect and 20% PVA + pTi in the meniscal-cartilage ROI at 14% of gait (Figure 5C) with forces of 179 ± 113 N, 278 ± 113 N, and 193 ± 96 N for the intact, defect, and 20% PVA + pTi respectively. A decrease in the total force between the intact knees and 20% PVA was found at 14% of gait in the cartilage-cartilage ROI, with the force in the intact condition averaging 359 ± 91 N of total force for the 7 knees tested and the 20% PVA having an average total forces of 295 ± 78 N (Figure 5D). At 45% of gait, there was a significant difference in total force between intact condition and the defect condition in the meniscal-cartilage contact area with average total force of 90 ± 73 N and 148 ± 75 N respectively (Figure 5C). Additionally, differences were found in the cartilage-cartilage total force at 45%

of gait between intact and all other conditions and between defect and 20% PVA + pTi (Figure 5D). The total forces were 486 ± 134 N for the intact, 360 ± 158 N for the defect, and 431 ± 177 for the 20% PVA + pTi, and the remaining implants tested having total force values below 412 N.

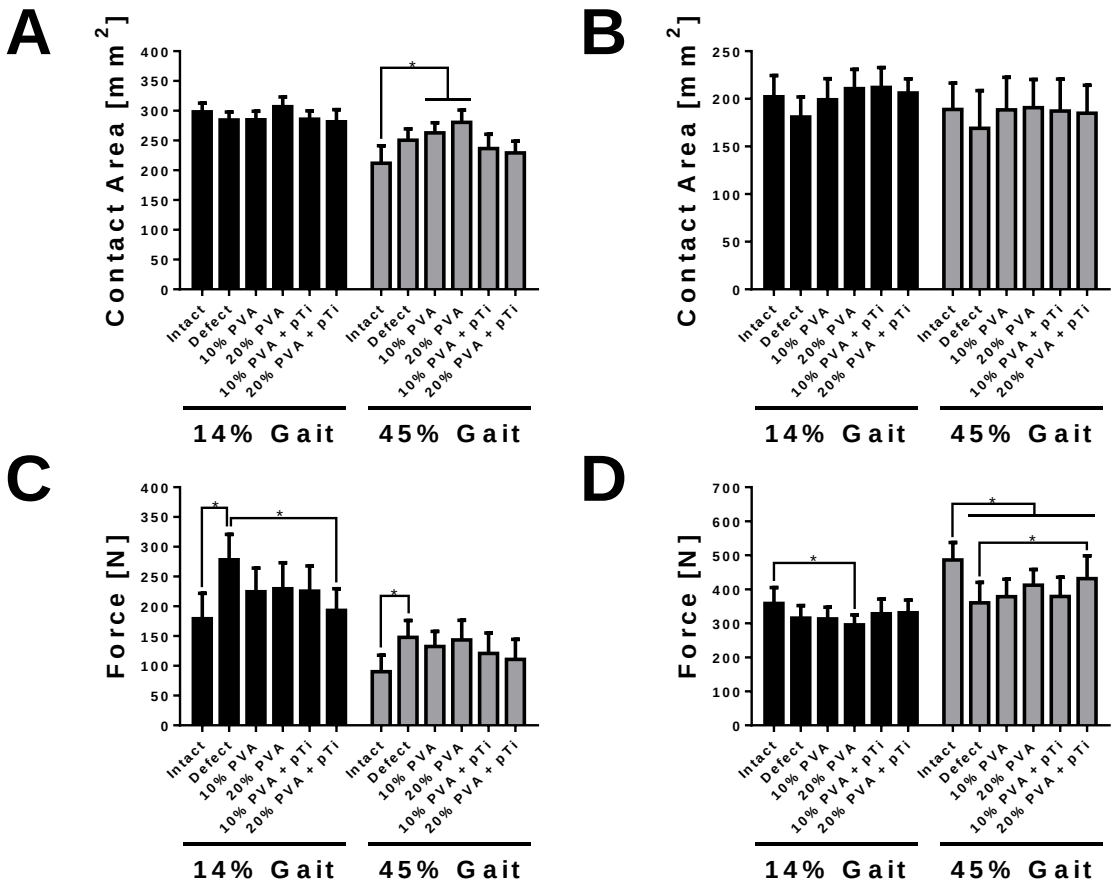

Figure 5: *Meniscal-Cartilage and Cartilage-Cartilage Contact Areas.* The contact area at 14% and 45% of the gait cycle in regions of A) meniscal-cartilage and B) cartilage-cartilage contact on the medial plateau. Meniscal-Cartilage and Cartilage-Cartilage Total Force. The total force at 14% and 45% of gait cycle in regions of C) meniscal-cartilage and D) cartilage-cartilage contact on the medial plateau. * represents significant differences between conditions ($p<0.05$).

Weighted Center of Contact Stress on the Medial Plateau

No differences were found between the WCoCS in either the M/L (Figure 6A) or A/P (Figure 6B) directions on the medial plateau.

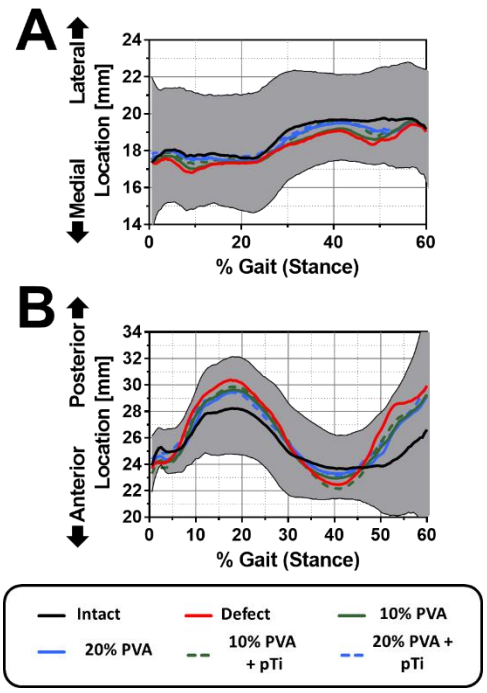

Figure 6: *Weighted Center of Contact Stress (WCoCS) through the Stance Phase of Gait.* The WCoCS in the A) medial/lateral and B) anterior/posterior directions on the medial plateau. Shaded region represents the 95% confidence intervals for the intact condition.

Stress Pattern Difference Maps

None of the test conditions were able to restore the total pattern differences back to the intact condition (Figure 7A&B). Additionally, no significant differences were seen between conditions.

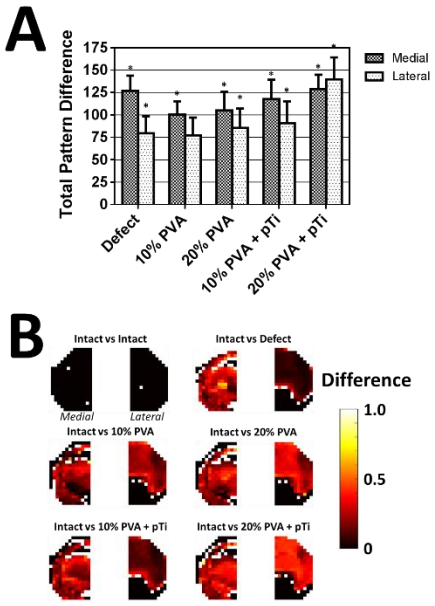

Figure 7: *Total Pattern Difference and Difference Maps*. A) Total pattern difference on the medial and lateral tibial plateaus. B) Representative pattern difference maps for all tested conditions. Note that the total pattern difference map for intact to intact is 0. * represents significant difference ($p<0.05$) from intact.

DISCUSSION

By testing the effects of osteochondral defects in a dynamic multidirectional simulator system, we have observed that the presence of a defect in areas of cartilage-cartilage contact caused redistribution of contact stress to the surrounding meniscus. Implants made from 20% PVAwith a pTi base, were able to partially restore the normal contact mechanics at 45% of gait in both the meniscal-cartilage and cartilage-cartilage zones. However, none of the tested conditions were able to reduce changes in stress patterns across the sensor suggesting that repair of osteochondral defects not only needs to take into consideration the mechanical properties of the repair but also the ability of the repair to restore normal joint contact mechanics.

The changes observed in the total force at 14% and 45% of gait contradict findings of a previously performed cadaveric loading model where stress was increases around the rim of the defect [4]. These discrepancies can be attributed to differences in loading conditions. In their system, only cartilage-on-cartilage contact is modeled; thus, when a defect is present, the load normally moderated by cartilage at the location of the defect is redistributed to the adjacent cartilage. In the present study, a similar phenomenon occurs, however, the cartilage is not solely responsible for redistribution of force with the meniscus also assuming a portion of the burden. This observation was also made using a finite element model created by Pena et al [25], where defects < 1 cm^2 did not have a large increase in force at the rim of the defect while defects > 1 cm^2 did. When the model was run with the medial meniscus removed, there was a substantial increase in defect rim forces regardless of the defect size suggesting that the meniscus plays a role in redistribution of loads when a focal defect is present. The increase in defect rim stresses in defects > 1 cm^2 indicates that the meniscus can no longer compensate for the lost surface area in those situations.

Interestingly, we observe minimal changes in total force and contact area in the cartilage-cartilage region at 14% of the gait cycle. The absence of changes in cartilage loading at this point in the gait cycle could be due to the fact that the meniscus carries an equal portion of the load whereas at 45% of gait, more load is carried by the cartilage [21]. When the load is redistributed in the presence of a focal articular cartilage defect at 14% of the gait cycle, the meniscus is engaged and capable of carrying more of the load whereas at 45% of the gait cycle the load is off-loaded more uniformly across the

plateau. Additionally, there were no differences in the WCoCS throughout the gait cycle suggesting that the force was still being distributed evenly across the plateau.

Stress pattern difference maps were generated to quantify local changes in contact stress. While the total stress was partially restored using the 20% PVA + pTi implants, these implants caused considerable changes in the contact stress patterns when compared to the intact condition. Surprisingly, when the analysis was performed on the lateral plateau similar stress patterns differences were seen. The stiffness of the implants, in conjunction with the fact that the implants protruded 0.2 mm above the surface of the articular cartilage, could explain the observed alterations in the lateral stress pattern differences. It is still unclear what changes in these loading patterns signify; however, it has been suggested that changes in stress patterns could lead to further degeneration in the surrounding cartilage caused by abrupt changes in contact mechanics that the cartilage cannot compensate for [26, 27].

We must take into account several limitations for the interpretation of these results. First, the simulator system does not control loading in the medial/lateral or varus/valgus directions. It would be important to test the effects of varus and valgus joint loading on the contact mechanics in the presence of a defect and with the different repairs; in normal gait kinematics there is a bias towards varus joint loading. Secondly, the electronic sensor can only measure contact stresses perpendicular to the articular surface. While the compressive load is an important predictor of future cartilage damage [28], another important factor in predicting early onset osteoarthritis are the changes in shear stress between the two opposing contact surfaces [29] which cannot currently be measured in this system. However, despite these limitations, the information obtained

using our cadaveric test system corroborates with finite element analysis of focal defects and provides a better understanding of the changes in joint contact mechanic that occur with an osteochondral defect and implant repair. This cadaveric testing system and analysis can ultimately be used as a testing platform for other repair technologies with future cadaveric experiments performed over a longer number of gait cycles to understand the effects of duty cycle on the performance of the implants and implants compared to allograft transplantation; a current treatment option for osteochondral defects.

REFERENCES

1. Brown TD, Pope DF, Hale JE, Buckwalter JA, Brand RA. Effects of osteochondral defect size on cartilage contact stress. J Orthop Res 1991; 9: 559-567.

2. Buckwalter JA, Anderson DD, Brown TD, Tochigi Y, Martin JA. The Roles of Mechanical Stresses in the Pathogenesis of Osteoarthritis: Implications for Treatment of Joint Injuries. Cartilage 2013; 4: 286-294.

3. Flanigan DC, Harris JD, Trinh TQ, Siston RA, Brophy RH. Prevalence of chondral defects in athletes' knees: a systematic review. Med Sci Sports Exerc 2010; 42: 1795-1801.

4. Flanigan DC, Harris JD, Brockmeier PM, Siston RA. The effects of lesion size and location on subchondral bone contact in experimental knee articular cartilage defects in a bovine model. Arthroscopy 2010; 26: 1655-1661.

5. Cole BJ, Pascual-Garrido C, Grumet RC. Surgical management of articular cartilage defects in the knee. Instr Course Lect 2010; 59: 181-204.

6. Khan IM, Gilbert SJ, Singhrao SK, Duance VC, Archer CW. Cartilage integration: evaluation of the reasons for failure of integration during cartilage repair. A review. Eur Cell Mater 2008; 16: 26-39.

7. Awad HA, Wickham MQ, Leddy HA, Gimble JM, Guilak F. Chondrogenic differentiation of adipose-derived adult stem cells in agarose, alginate, and gelatin scaffolds. Biomaterials 2004; 25: 3211-3222.

8. Chen T, Hilton MJ, Brown EB, Zuscik MJ, Awad HA. Engineering superficial zone features in tissue engineered cartilage. Biotechnol Bioeng 2013; 110: 1476-1486.

9. Huang AH, Farrell MJ, Kim M, Mauck RL. Long-term dynamic loading improves the mechanical properties of chondrogenic mesenchymal stem cell-laden hydrogel. Eur Cell Mater 2010; 19: 72-85.

10. Mauck RL, Nicoll SB, Seyhan SL, Ateshian GA, Hung CT. Synergistic action of growth factors and dynamic loading for articular cartilage tissue engineering. Tissue Eng 2003; 9: 597-611.

11. Ng KW, Mauck RL, Wang CC, Kelly TA, Ho MM, Chen FH, et al. Duty Cycle of Deformational Loading Influences the Growth of Engineered Articular Cartilage. Cell Mol Bioeng 2009; 2: 386-394.

12. Allan KS, Pilliar RM, Wang J, Grynpas MD, Kandel RA. Formation of biphasic constructs containing cartilage with a calcified zone interface. Tissue Eng 2007; 13: 167-177.

13. Khanarian NT, Haney NM, Burga RA, Lu HH. A functional agarose-hydroxyapatite scaffold for osteochondral interface regeneration. Biomaterials 2012; 33: 5247-5258.

14. O'Shea TM, Miao X. Bilayered scaffolds for osteochondral tissue engineering. Tissue Eng Part B Rev 2008; 14: 447-464.

15. St-Pierre JP, Gan L, Wang J, Pilliar RM, Grynpas MD, Kandel RA. The incorporation of a zone of calcified cartilage improves the interfacial shear strength between in vitro-formed cartilage and the underlying substrate. Acta Biomater 2012; 8: 1603-1615.

16. Baker MI, Walsh SP, Schwartz Z, Boyan BD. A review of polyvinyl alcohol and its uses in cartilage and orthopedic applications. J Biomed Mater Res B Appl Biomater 2012; 100: 1451-1457.

17. Ng KW, Wanivenhaus F, Chen T, Hsu HC, Allon AA, Abrams VD, et al. A novel macroporous polyvinyl alcohol scaffold promotes chondrocyte migration and interface formation in an in vitro cartilage defect model. Tissue Eng Part A 2012; 18: 1273-1281.

18. Scholten PM, Ng KW, Joh K, Serino LP, Warren RF, Torzilli PA, et al. A semi-degradable composite scaffold for articular cartilage defects. J Biomed Mater Res A 2011; 97: 8-15.

19. Oka M, Ushio K, Kumar P, Ikeuchi K, Hyon SH, Nakamura T, et al. Development of artificial articular cartilage. Proc Inst Mech Eng H 2000; 214: 59-68.

20. Bedi A, Chen T, Santner TJ, El-Amin S, Kelly NH, Warren RF, et al. Changes in dynamic medial tibiofemoral contact mechanics and kinematics after injury of the anterior cruciate ligament: a cadaveric model. Proc Inst Mech Eng H 2013; 227: 1027-1037.

21. Gilbert S, Chen T, Hutchinson ID, Choi D, Voigt C, Warren RF, et al. Dynamic contact mechanics on the tibial plateau of the human knee during activities of daily living. J Biomech 2014; 47: 2006-2012.

22. Wang H, Gee AO, Hutchinson ID, Stoner K, Warren RF, Chen TO, et al. Bone Plug Versus Suture-Only Fixation of Meniscal Grafts: Effect on Joint Contact Mechanics During Simulated Gait. Am J Sports Med 2014; 42: 1682-1689.

23. Holloway JL, Lowman AM, Palmese GR. Aging behavior of PVA hydrogels for soft tissue applications after in vitro swelling using osmotic pressure solutions. Acta Biomater 2013; 9: 5013-5021.

24. DesJardins JD, Walker PS, Haider H, Perry J. The use of a force-controlled dynamic knee simulator to quantify the mechanical performance of total knee replacement designs during functional activity. J Biomech 2000; 33: 1231-1242.

25. Pena E, Calvo B, Martinez MA, Doblare M. Effect of the size and location of osteochondral defects in degenerative arthritis. A finite element simulation. Comput Biol Med 2007; 37: 376-387.

26. Andriacchi TP, Mundermann A. The role of ambulatory mechanics in the initiation and progression of knee osteoarthritis. Curr Opin Rheumatol 2006; 18: 514-518.

27. Chaudhari AM, Briant PL, Bevill SL, Koo S, Andriacchi TP. Knee kinematics, cartilage morphology, and osteoarthritis after ACL injury. Med Sci Sports Exerc 2008; 40: 215-222.

28. Dabiri Y, Li LP. Altered knee joint mechanics in simple compression associated with early cartilage degeneration. Comput Math Methods Med 2013; 2013: 862903.

29. Setton LA, Elliott DM, Mow VC. Altered mechanics of cartilage with osteoarthritis: human osteoarthritis and an experimental model of joint degeneration. Osteoarthritis Cartilage 1999; 7: 2-14.